Rock Mechanics and Rock Engineering (2020) 53:4787–4798
https://doi.org/10.1007/s00603-020-02175-3

TECHNICAL NOTE

A New Dynamic Direct Shear Testing Device on Rock Joints

Shengwen Qi[1,2,3] · Bowen Zheng[1,2,3] · Faquan Wu[4] · Xiaolin Huang[1,2,3] · Songfeng Guo[1,2,3] · Zhifa Zhan[5] · Yu Zou[1,2,3] · Giovanni Barla[6]

Received: 17 January 2020 / Accepted: 9 June 2020 / Published online: 1 July 2020

Keywords Direct shear · Dynamic load · Cyclic load · New apparatus · Constant normal load · Constant normal stiffness

1 Introduction

Discontinuities, i.e., joints, bedding planes, contacts and faults (ISRM 2007), are widely developed in rock masses. The assessment of the shear strength of these discontinuities is very important for evaluating the stability of rock structures, so lots of researches have been carried out on this aspect (i.e., Patton 1966; Barton 1973; Barton and Choubey 1977; Grasselli and Egger 2003; Guo and Qi 2015; Zheng and Qi 2016). In addition to static shear loads, also dynamic shear loads, e.g., seismic wave loads, which are rapid and cyclic loads, need to be considered (i.e., Li et al. 2011, 2014).

The shear strength of discontinuities under dynamic cyclic shearing is expected to decrease gradually (i.e., Crawford and Curran 1981). Therefore, a rock structure which is stable under static loads may move or slide along the discontinuities and co-seismic landslides or other instabilities may occur during strong earthquakes (i.e., Qi et al. 2010, 2011, 2015). Hence, the shear behavior of discontinuities under dynamic cyclic shearing should be properly investigated (Dang et al. 2016; Fathi et al. 2016).

✉ Shengwen Qi
qishengwen@mail.iggcas.ac.cn

1 Key Laboratory of Shale Gas and Geoengineering, Institute of Geology and Geophysics, Chinese Academy of Sciences, Beijing, China

2 Innovation Academy for Earth Science, Chinese Academy of Sciences, Beijing, China

3 University of Chinese Academy of Sciences, Beijing, China

4 Shaoxing University, Shaoxing, China

5 China Highway Engineering Consulting Corporation, Beijing, China

6 Politecnico di Torino, Torino, Italy

Laboratory shear testing has been widely used to investigate the shear behavior of discontinuities under different shear rate conditions (Schneider 1977; Crawford and Curran 1981; Li et al. 2006; Mehrishal et al. 2016; Kleepmek et al. 2016). The dynamic direct shear apparatus used to test the dynamic shear behavior of discontinuities is significantly different from the static direct shear apparatus adopted in the references i.e., Cen and Huang (2017), Huang and Zhu (2018), Zhu and Huang (2019).

In addition to the basic equipment, i.e., the normal and tangential loading devices, the shear box, the hydraulic control device and the data acquisition and processing system (Barla et al. 2010; Huang and Zhu 2019), a servo oil source system with a large flow and accumulator is needed. The maximal shear rate and frequency are requested to be in the range 600–1000 mm/s and 10–20 Hz, respectively (Hu et al. 1996). At the same time, the specimens should be large enough to simulate the seismic wave loads properly as suggested by Barton and Choubey (1977), with a maximal length of at least 100–1000 mm.

Typical direct shear apparatuses for dynamic shear in the laboratory are shown in Table 1 and Fig. 1. It is noted that the specimen size in the dynamic direct shear apparatuses of the University of Toronto (Crawford and Curran 1981) and of the Université Joseph Fourier (Hans and Boulon 2003) and the shear rate (shear strain rate) in the dynamic direct shear apparatuses of the Technische Universität Bergakademie Freiberg (Konietzky et al. 2012) cannot meet the requirement of the seismic wave loads (Fig. 1). These are also the cases of the dynamic direct shear apparatus of the Institute of Rock and Soil Mechanics, Chinese Academy of Sciences (Li et al. 2006) and of the University of Wollongong (Indraratna et al. 1998). Especially no device can carry out the authentic seismic wave loads in both the normal and tangential directions (Table 1).

Table 1 Index parameters of representative dynamic direct shear apparatuses

Organizations with dynamic direct shear apparatuses	Maximal specimen size (mm)	Shear rate (mm/s)	Seismic wave loading	Constant normal stiffness condition
Institute of Rock and Soil Mechanics, Chinese Academy of Sciences, China (Li et al. 2006)	150 × 150	0.0001–1	None	None
University of Toronto, Canada (Crawford and Curran 1981)	300 × 200	0.05–200	None	None
University of Wollongong, Australia (Indraratna et al. 1998)	250 × 75	0–20	None	Spring control
Université Joseph Fourier, France (Hans and Boulon 2003)	100 × 100	0.05–500	In the tangential direction	Servo control
Technische Universität Bergakademie Freiberg, Germany (Konietzky et al. 2012)	400 × 200	0–70	In the normal direction	Servo control
Institute of Geology and Geophysics, Chinese Academy of Sciences, China (The new device in this paper)	1000 × 250	0.001–1000	In both the normal and tangential directions	Servo control

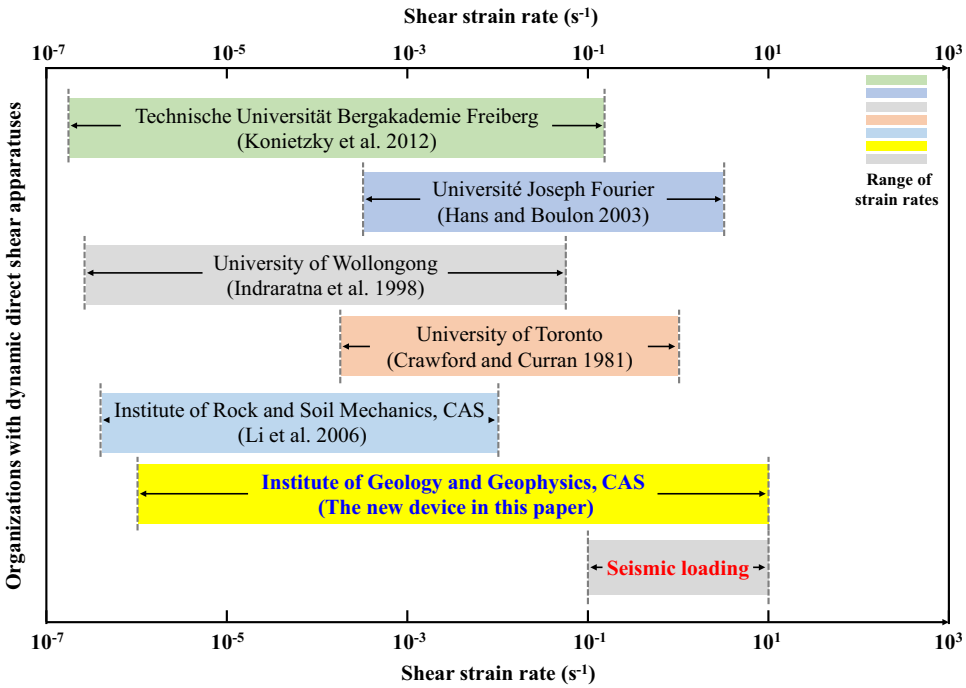

Fig. 1 Range of shear strain rates of typical direct shear apparatuses for dynamic shear (For interpretation of the references to colour in this figure legend, the reader is referred to the web version of this paper)

Therefore, the lack of an accurate laboratory dynamic direct shear test system for discontinuities is a bottleneck for elucidating the dynamic shear behavior of discontinuities subject to the seismic wave loads. To remove this limitation, a new dynamic direct shear testing device on rock joints (TFD-500/1000-JS, Table 1 and Fig. 1) is introduced in the following, where the performance of the new testing device and some applications will be briefly presented.

2 New Dynamic Direct Shear Testing Device

2.1 Hardware and Software

The new device comprises normal and tangential loading devices, shear box, hydraulic control system, and data acquisition and processing devices, in addition to

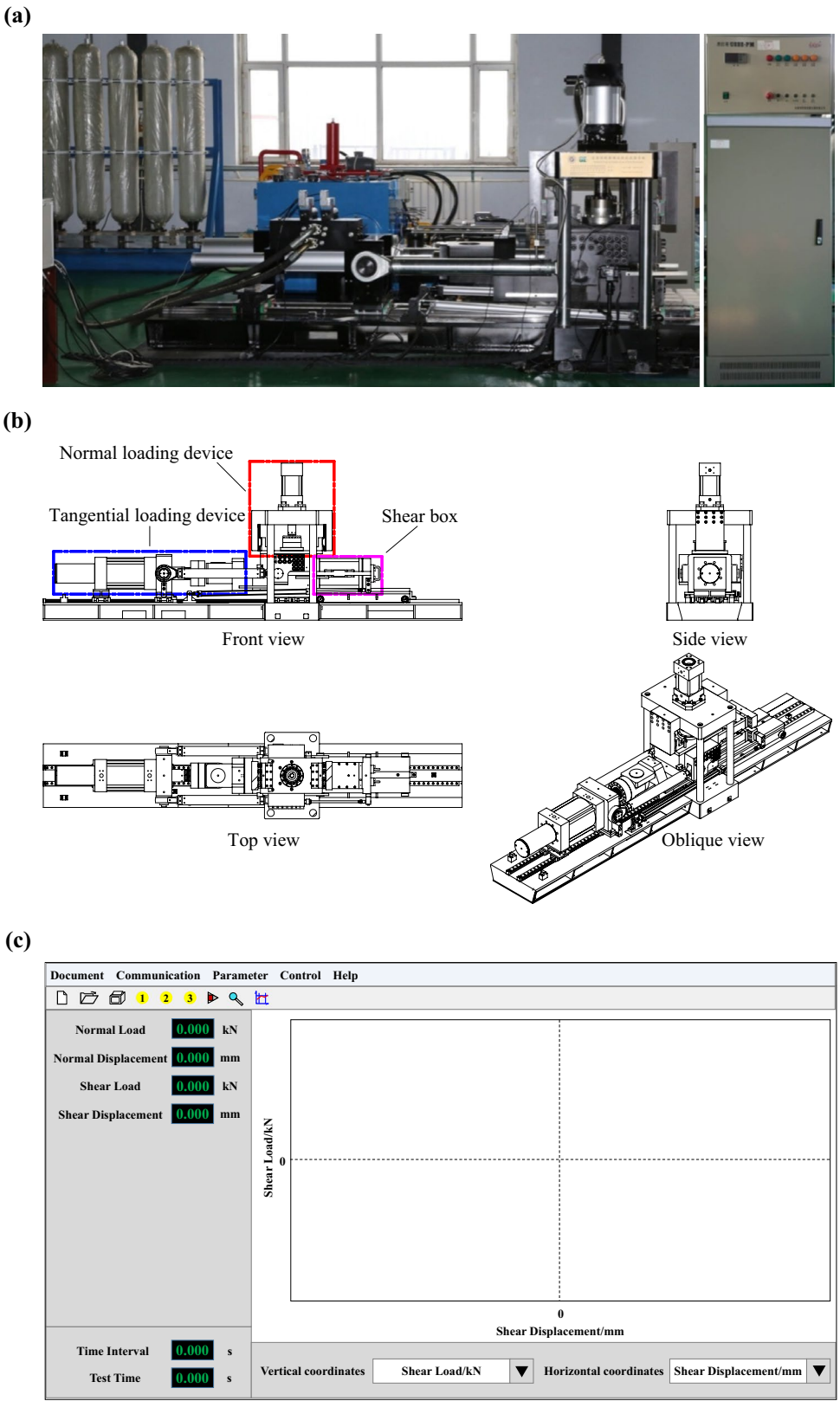

Fig. 2 Hardware and software schemes of the new testing device. **a** Testing device. **b** Mainframe. **c** Interface. **d** Loading moduli

Fig. 2 (continued)

(d)

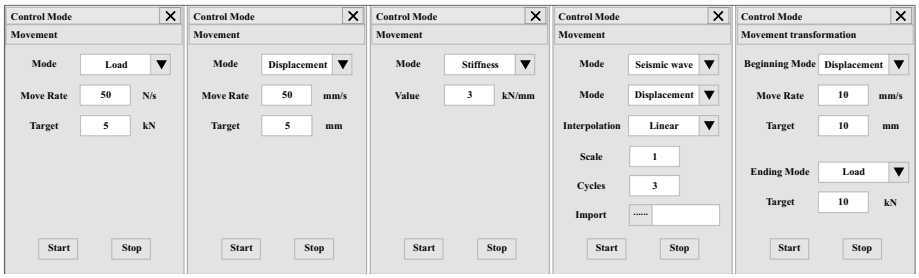

auxiliary hardware, as shown in Fig. 2a, b. The normal loading device consists of a normal hydrocylinder and a normal servo valve, and the maximal pressure of the normal hydrocylinder that can be achieved is 500 kN. The tangential loading device includes tangential hydrocylinders and tangential servo valves. Two tangential hydrocylinders are included, i.e., a large hydrocylinder and a small hydrocylinder, which can be switched according to the test requirements. The maximal loading capacities of the tangential large and small hydrocylinders are 1000 kN and 100 kN, respectively.

The shear box is composed of an upper shear box and a lower shear box. The hydraulic control device mainly includes an oil source, an accumulator and a control system. The data acquisition and processing devices mainly consist of normal and tangential load sensors, normal and tangential displacement sensors. The normal load sensor has a 500 kN full scale with a 2.8 N resolution ratio, and the tangential load sensors have full ranges of 1000 kN with a resolution ratio of 5.6 N and of 100 kN with a 0.56 N resolution ratio for the large and small hydrocylinders, respectively. The normal and tangential displacement sensors have full scales of ± 75 mm and ± 200 mm with a resolution ratio of 1 μm, respectively.

The internal length of the shear box ranges from 100 mm to 1000 mm. The scale of the normal loading rate is from 0.001 mm/s to 100 mm/s, and the ranges of shear rate are from 0.001 mm/s to 100 mm/s and from 0.001 mm/s to 1000 mm/s for the large and small hydrocylinders, respectively. The shear displacement/loading frequency ranges from 0 Hz to 20 Hz. The device can apply the seismic wave loads in both the normal and tangential directions, and all the index parameters of the new testing device are in accordance with the requirements of the dynamic direct shear tests as suggested by Barton and Choubey (1977) and Hu et al. (1996) (Fig. 1 and Table 1).

The loading moduli of the operating software includes the load control mode, the displacement control mode, and the stiffness control mode, as shown in Fig. 2c, d. The initial test parameters are preset via the device operating software, and then the curves of the normal load, the shear load, the normal displacement, the shear displacement and other parameters varying with time are generated during the test. Based on the test curves, the testing process is set in real time.

2.2 Operating Principles

The specimen is first placed in the shear box. The vertical and horizontal displacements are governed by the upper and lower shear boxes, respectively. After turning on the control device (and software) and the oil source (including the accumulator), the initial normal load, the normal stiffness, and the shear displacement parameters are preset and the shear mode is selected.

Subsequently, the initial normal load is applied to the specimen through the upper shear box from the oil source, the normal servo valve and the normal hydrocylinder. The normal load is then controlled in real time during the test according to the pre-set testing conditions. Similarly, the shear load is applied via the lower shear box by using the oil source, the tangential servo valve and the tangential hydrocylinder. The shear loading is stopped when the shear displacement reaches the pre-set value. Finally, the load and specimens are removed.

During the test, the real-time values of the normal and shear loads, the normal and shear displacements are recorded by the sensors and fed back to the control device (and software). The operating software gives the parameters that are required for the test and the load and displacement values are stored. The entire test process forms a servo-closed loop with characteristics of good controllability and high stability, as shown in Fig. 3.

2.3 Key Technologies

There are four key technologies of the new testing device: dynamic and cyclic loading, servo closed-loop constant normal stiffness loading, multiscale model testing and high-resolution detection. These are briefly described in the following.

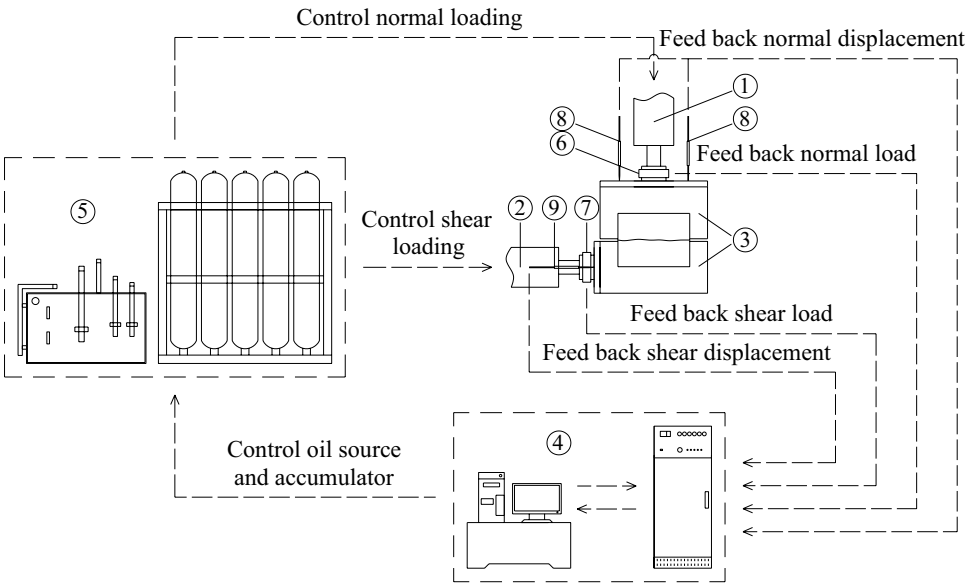

Fig. 3 Operating principle of the new testing device

Structure name: ①Normal hydrocylinder ②Tangential hydrocylinder ③Shear box ④Computer and control device ⑤Oil source and accumulator ⑥Normal load sensor ⑦Tangential load sensor ⑧Normal displacement sensors ⑨Tangential displacement sensors

2.3.1 Dynamic and Cyclic Loading

The new testing device is equipped with a high-energy oil source with a large flow and accumulator to provide a strong driving force, which allows one to obtain the dynamic and cyclic loading process with various rates, frequencies and amplitudes in both the normal and tangential directions. The loading modes include various wave loads, such as the strong seismic wave load, the random wave load, the triangular wave load, and the simple harmonic wave load.

The loading modes for earthquakes are set as follows: (1) the real seismic record is collected and revised (e.g., baseline correction); (2) the corresponding acceleration versus time curve record after revision is integrated twice and the displacement versus time curve obtained. Then, the discrete points of the displacement versus time curve are derived and input into the operating software to apply the strong seismic wave load (Fig. 4a, b). Taking the tangential loading as an example, the triangular and superposed harmonic wave loading modes with various frequencies and amplitudes are given in Fig. 4c, d.

2.3.2 Servo Closed-Loop Constant Normal Stiffness Loading

A shear test under both the constant normal load (CNL) and constant normal stiffness (CNS) conditions can be performed in a servo closed loop control mode. For example, if reference is made to a CNS test, the shear dilatancy of an irregular undulated discontinuity is recorded by the normal displacement sensors in real time and fed back to the control device. Then, the real-time normal load increment is obtained based on the normal displacement Δy multiplied by the normal stiffness k_n.

Next, the initial normal load and the increased normal load controlled by the normal hydrocylinder are applied on the specimen via the oil source and the normal servo valve. In other words, the normal load of the specimen in real time $P_n\ (t+\Delta t)$ is the sum of the initial normal load $P_n\ (t)$ and the increased normal load ΔP_n, as shown in Eqs. (1) and (2) (Jiang et al. 2004; Hans and Boulon 2003):

$$\Delta P_n = k_n \times \Delta y \tag{1}$$

$$\Delta P_n(t+\Delta t) = \Delta P_n(t) + \Delta P_n \tag{2}$$

where k_n is the normal stiffness, Δy is the normal displacement increment, ΔP_n is the normal load increment, Δt is the time interval, $P_n\ (t)$ is the normal load at time t, and $P_n\ (t+\Delta t)$ is the normal load at time $t+\Delta t$.

2.3.3 Multiscale Model Testing

The internal dimension of the shear box of the new testing device is adjustable given the particular structural design that allows for removing and installing different accessories. In detail, the upper and lower shear boxes can be set to different sizes so that the length of the upper discontinuity

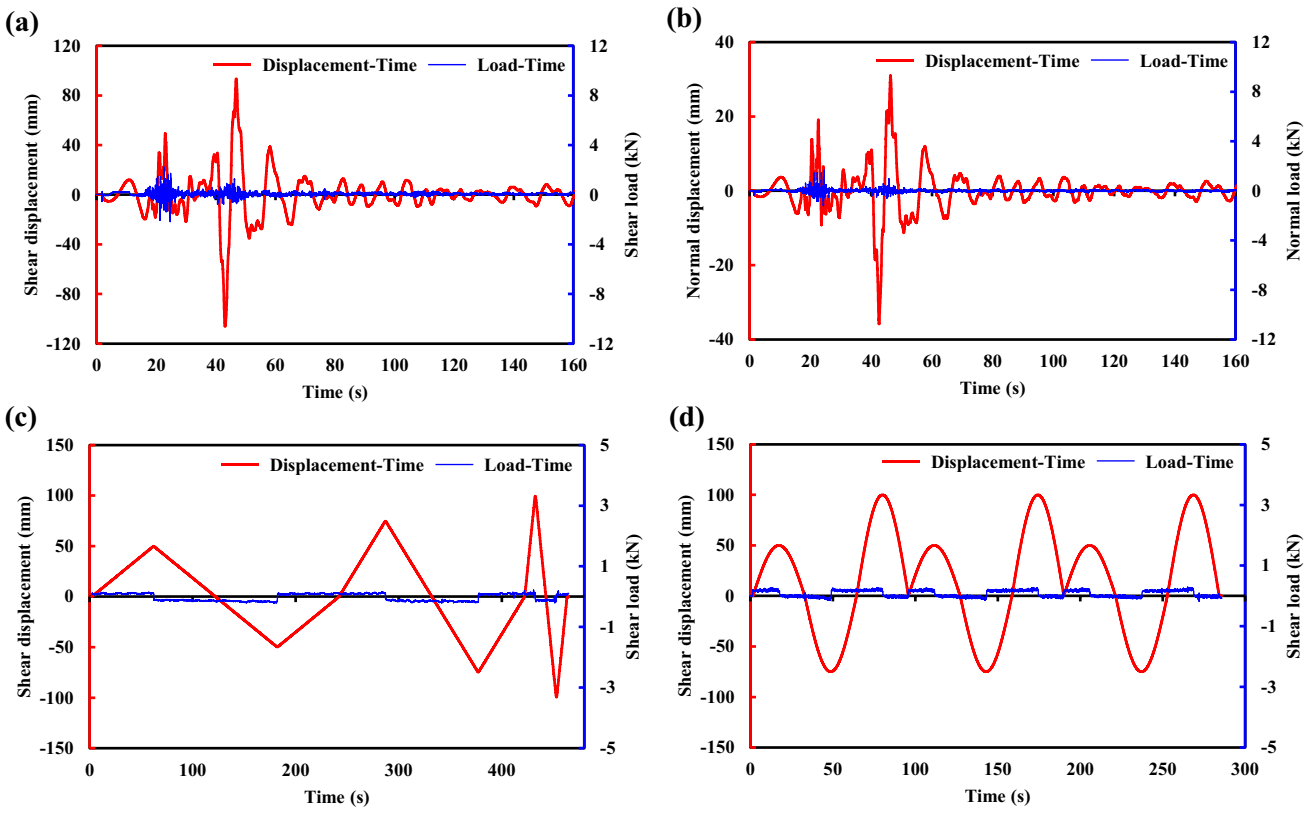

Fig. 4 Inputs for the displacement versus time of a strong seismic wave load, a triangular wave load and a superposed harmonic wave load. **a** Loading inputs transformed from a seismic record of the Wenchuan earthquake, China, on May 12, 2008, in the tangential direction and corresponding shear load versus time curve. **b** Reduced tangential directional loading inputs in the normal direction and corresponding normal load versus time curve. **c** Triangular loading inputs with various frequencies and amplitudes in the tangential direction and corresponding shear load versus time curve. **d** Superposed harmonic loading inputs with various frequencies and amplitudes in the tangential direction and corresponding shear load versus time curve (For interpretation of the references to colour in this figure legend, the reader is referred to the web version of this paper)

specimen in the upper shear box can be smaller than that in the lower shear box.

The design that considers the size difference of the upper and lower shear boxes as well as a large shear displacement, up to 400 mm, can maintain a constant area between the upper and lower discontinuity surfaces during the dynamic and cyclic shear process under high-rate and large-amplitude conditions.

Moreover, the tangential large and small hydrocylinders are suitable for the low-rate shear test of a large-scale specimen and the high-rate shear test of a small-scale specimen, respectively. This allows one to take into account the dynamic shear strength of the discontinuities.

2.3.4 High-Resolution Detection

The new testing device is equipped with four linear variable differential transducers (LVDTs) to measure the normal displacement and two LVDTs for the shear displacement. Moreover, the device is equipped with a high-speed camera (Pco. Dimax. HS1) and a 3D laser scanner (Creaform Viuscan) that can be used to observe the crack propagation process to allow for the description of the dynamic shear behavior and the changes in the morphology of the discontinuities before and after the shear test.

As described above, compared with the dynamic direct shear apparatuses listed in Table 1, the new testing device overcomes the limitations of the existing apparatuses with reference to the internal dimension of the shear box, the shear rate range and the CNS shear condition. In particular, the seismic wave loads in both the normal and tangential directions can be applied, including large shear displacements. The mechanical properties of discontinuities subject to the strong seismic wave loads can be measured conveniently and more accurately compared to the existing apparatuses. These advantages allow properly studying the dynamic mechanical properties of rock discontinuities.

3 Operation of the New Testing Device

To illustrate the feasibility and the reliability, a number of laboratory tests have been performed with the new device. Examples of both static and dynamic shear tests are briefly introduced in the following.

3.1 Static Direct Shear Tests on Intact Gypsum Specimens

To test the static loading performance of the new testing device, static direct shear tests (with a shear strain rate less than 10^{-4}/s) were carried out on intact gypsum specimens, formed with high-strength gypsum, water and fly ash. Fly ash could reduce the bubbles generated during preparation. The mass ratio of gypsum, water and fly ash was 175:70:2.

The specimen preparation process was as follows: First, butter was smeared over a mold with a dimension of 100 mm × 100 mm × 100 mm. The materials were mixed and stirred thoroughly, and then poured into the mold. Via vibration and tamping processes, the specimen was demolded after 1 h. Finally, the same specimen was held at the room temperature for 28 days. Seven gypsum specimens (numbered one to seven), were prepared for testing.

Static direct shear tests of same loading conditions on the seven gypsum specimens were performed under the CNL condition with 5 kN being applied at a rate of 50 N/s and then remained constant. Then, the shear load was applied in the displacement control mode at a rate of 0.005 mm/s, corresponding to a shear strain rate of

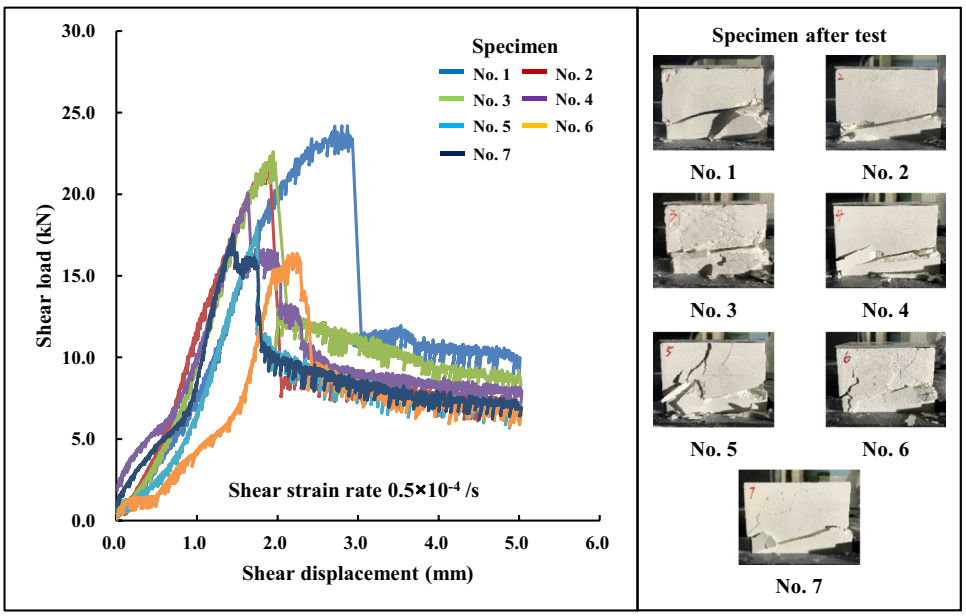

Fig. 5 Intact gypsum specimens and shear load versus shear displacement curves (For interpretation of the references to colour in this figure legend, the reader is referred to the web version of this paper)

Table 2 Test parameters of the intact gypsum specimens

Specimen No.	Normal load (kN)	Shear strain rate (/s)	Peak shear load (kN)	Residual shear load (kN)	Peak shear displacement (mm)	Shear stiffness (kN/mm)	Difference between peak and residual shear load (kN)
1	5	0.5×10^{-4}	24.192	10.806	2.802	15.549	13.386
2			21.94	8.057	1.892	17.844	13.883
3			22.584	9.61	1.947	16.466	12.974
4			20.046	8.752	1.634	17.574	11.294
5			17.991	7.681	1.741	15.967	10.31
6			16.381	7.664	2.241	20.54	8.717
7			17.575	7.954	1.445	22.912	9.621
Average value			20.101	8.646	1.957	18.122	11.455
Standard deviation			2.914	1.178	0.449	2.683	2.005
Coefficient of variation (Dimensionless)			14.497	13.625	22.932	14.805	17.503

0.5×10^{-4}/s until the shear displacement reached the pre-set value. The shear load versus shear displacement curves of the seven tests performed and the photos following shear failure are shown in Fig. 5.

Figure 5 shows that spalling takes place in some parts of the specimens involving portions of the surface. The shear load versus shear displacement curves exhibit an elastic-brittle response. According to Fig. 5, the test parameters, such as the peak shear load, the peak shear displacement, the shear stiffness, and the residual shear load, are given in Table 2 with the mean, standard deviation and coefficient of variation values. The differences observed in both the fracture patterns and test parameters are possibly due to the deviations of specimen preparation, which result in the differences of surficial flatness and internal compactness of the gypsum specimens.

3.2 Dynamic Direct Shear Tests on the Granite Specimen with One Joint

Dynamic direct shear tests with a shear strain rate greater than 10^{-4}/s were performed on the granite specimen with a planar joint shown in Fig. 6a, b. The dimensions of the top and bottom blocks were 100 mm × 55 mm × 100 mm and 200 mm × 55 mm × 100 mm, respectively. These blocks were placed in the upper and lower shear boxes for testing.

Dynamic direct shear tests were carried out under a constant normal load of 5 kN. During the process of each test, the normal load was applied first at a rate of 50 N/s and then held constant. The shear load was exerted in the displacement control mode at a rate ranging between 0.01 mm/s and 1000 mm/s, i.e., a shear strain rate ranging between 1×10^{-4}/s and 1×10/s until the shear displacement reached the pre-set value. In order to collect the test data as many as possible, we increased the sampling frequency with the increase of the shear rate during the tests. Specifically, the

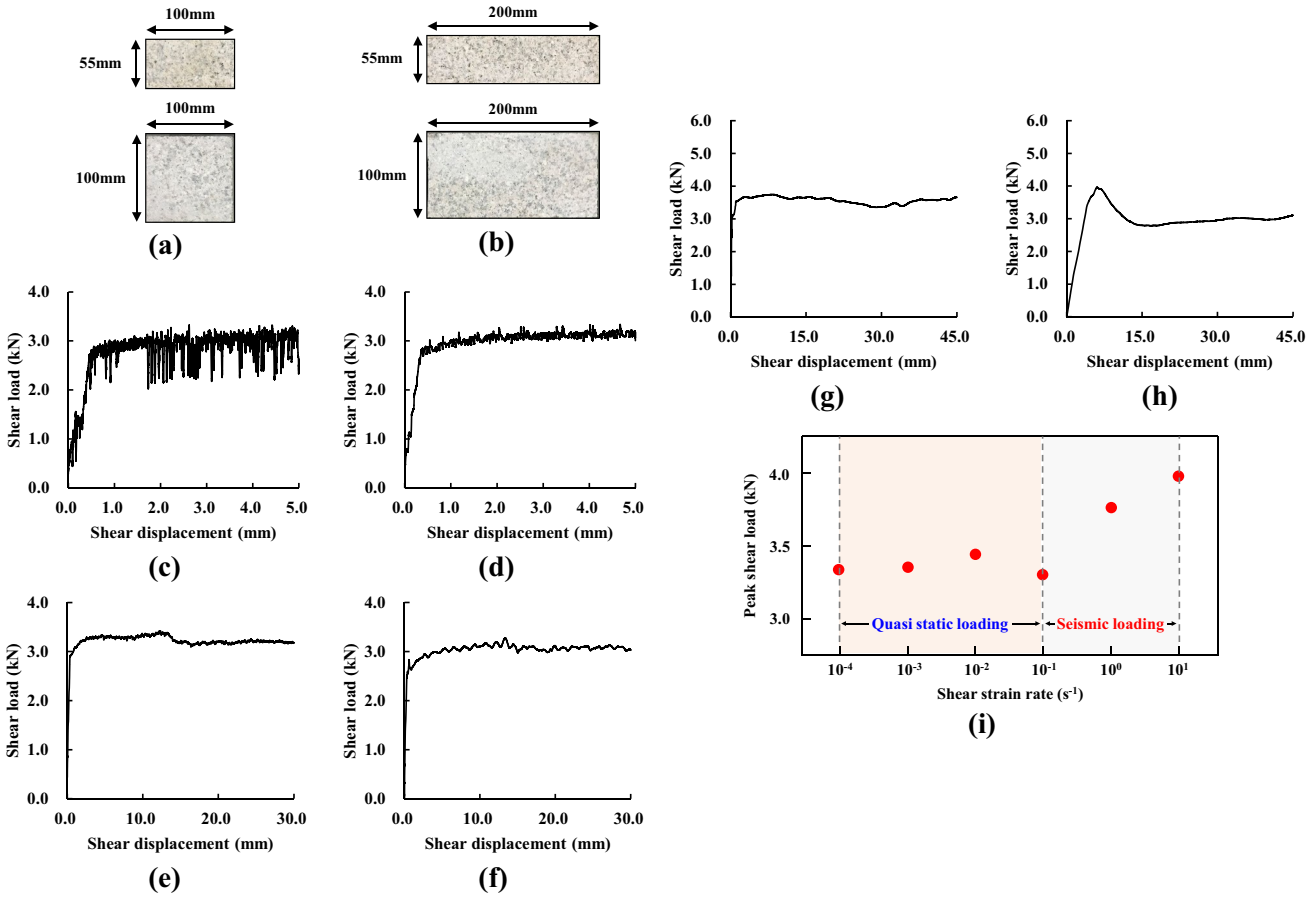

Fig. 6 The granite specimen with a joint and shear load versus shear displacement curves. **a** The side view and top view of the top block. **b** The side view and top view of the bottom block. **c** A test curve under a shear strain rate of 1×10^{-4}/s. **d** A test curve under a shear strain rate of 1×10^{-3}/s. **e** A test curve under a shear strain rate of 1×10^{-2}/s. **f** A test curve under a shear strain rate of 1×10^{-1}/s. **g** A test curve under a shear strain rate of 1/s. **h** A test curve under a shear strain rate of 1×10/s. **i** Variation of the peak shear load versus the shear strain rate

sampling frequency was set as 1000 Hz in the test at a rate of 1000 mm/s (1 × 10/s). The shear load versus shear displacement curves are shown in Fig. 6c–h.

Figure 6c–g indicate that the joint shows a perfectly elastic-plastic behavior under dynamic shearing with the strain rate ranging between 1×10^{-4}/s and 1/s. While the shear strain rate reaches 1 × 10/s, the joint shows an obviously strain-softening behavior, and there is a peak value following post-peak residual stage on the shear load versus shear displacement curve as shown in Fig. 6h. Additionally, the fluctuations that may result from the stick-slip behavior can be observed on the test curves in Fig. 6c–f, which gradually disappear as the shear rate increases, i.e., Fig. 6g, h. Meanwhile, the shear resistance (the peak shear load) increases with the increase of the shear strain rate in the range of $1 \times 10^{-4} \sim 1 \times 10^{1}$/s, especially in the range of $1 \times 10^{-1} \sim 1 \times 10^{1}$/s (seismic wave loads) (Fig. 6i). In other words, the shear behavior of the joint has an obvious shear strain rate dependency, especially in the range of $1 \times 10^{-1} \sim 1 \times 10^{1}$/s (seismic wave loads).

Additionally, to demonstrate the key technique of "cyclic loading", the cyclic shear test results of the granite joint with

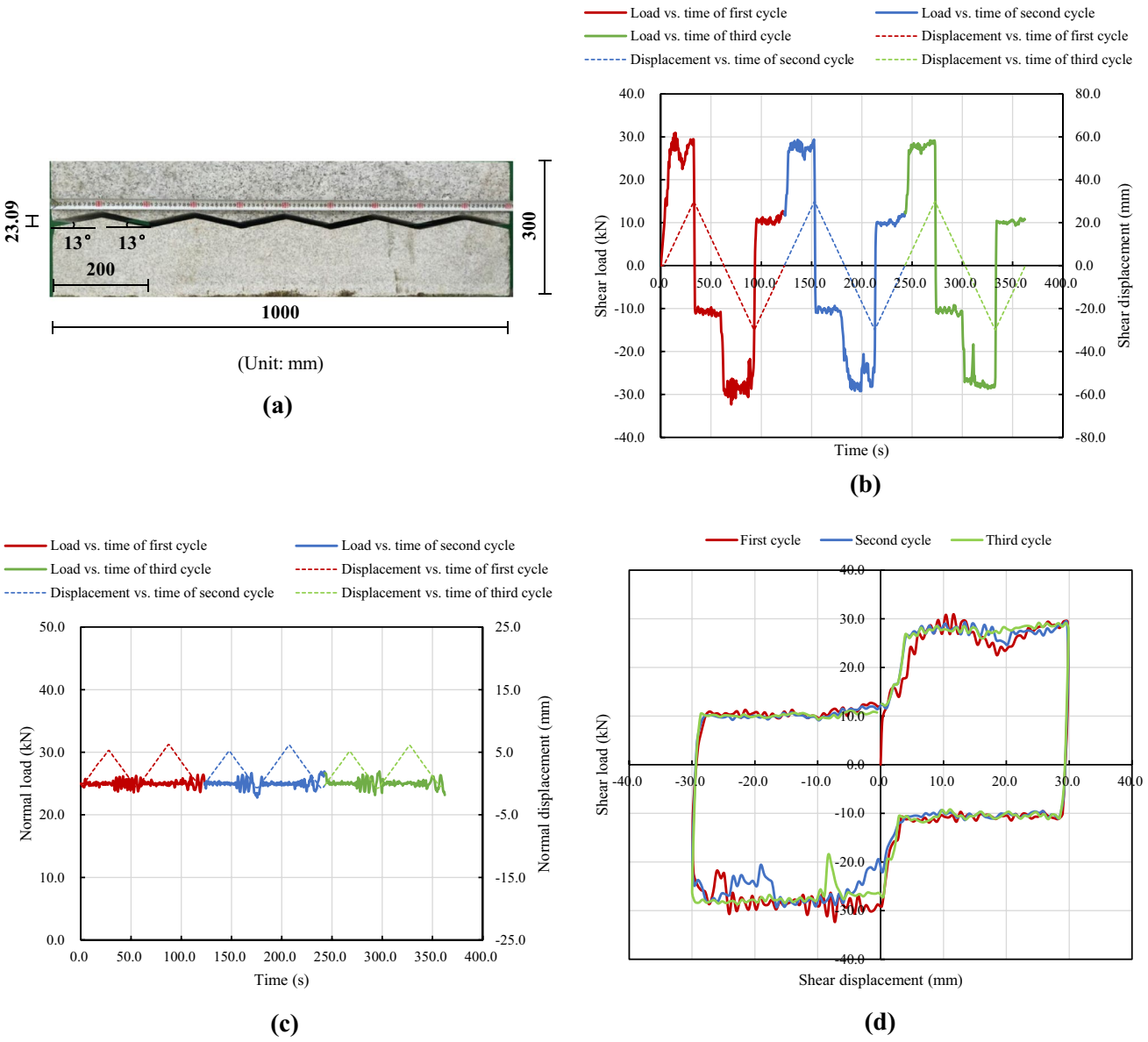

Fig. 7 The example of cyclic shear test results under the CNL condition. **a** The schematic diagram of the granite joint with the regular sawtooth shape (front view). **b** Shear load and shear displacement versus time curves. **c** Normal load and normal displacement versus time curves. **d** Shear load versus shear displacement curves (For interpretation of the references to colour in this figure legend, the reader is referred to the web version of this paper)

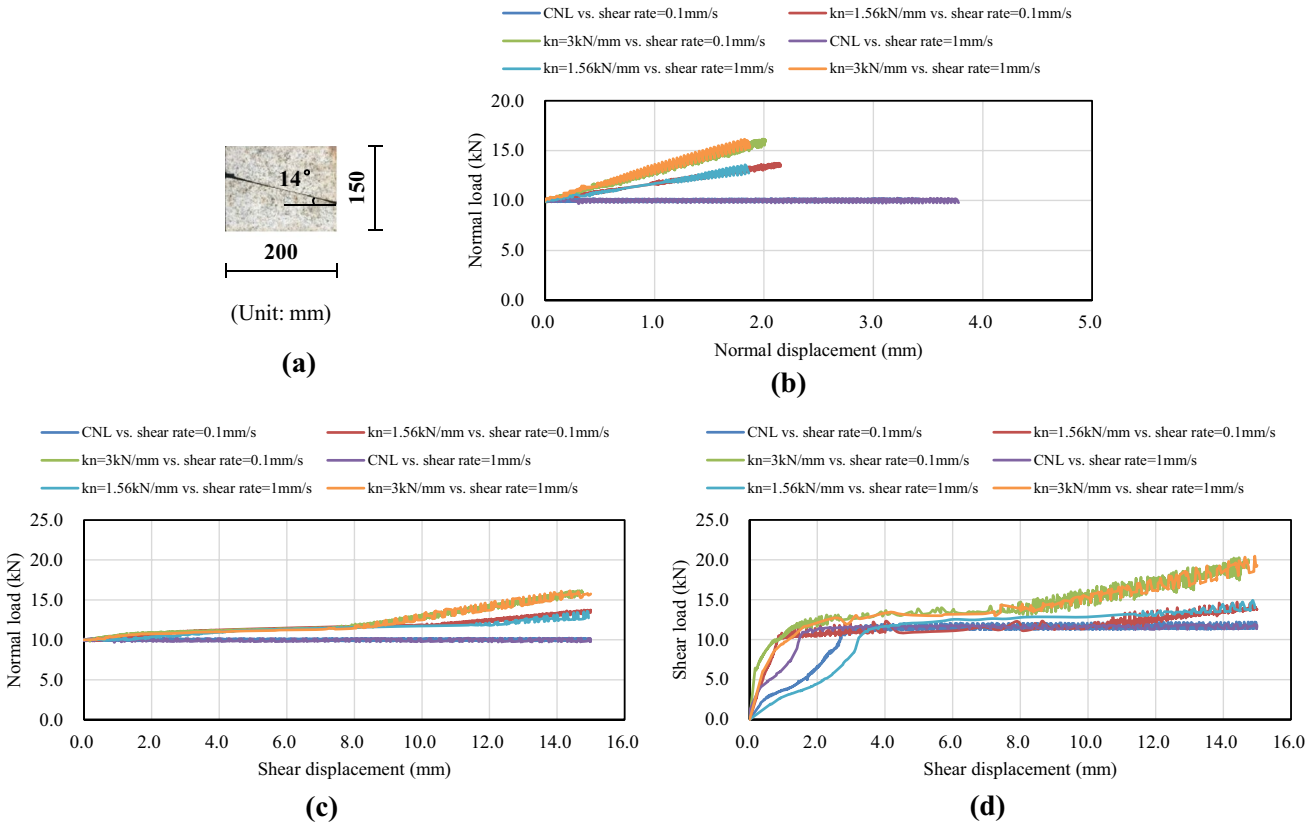

Fig. 8 The example of shear test results under the CNS condition. **a** The schematic diagram of the granite joint with the tilted flat and straight shape (front view). **b** Normal load versus normal displacement curves. **c** Normal load versus shear displacement curves. **d** Shear load versus shear displacement curves (For interpretation of the references to colour in this figure legend, the reader is referred to the web version of this paper)

the specimen length of 1000 mm under the CNL condition, is shown in Fig. 7 of "Appendix". To reflect the key technique of "CNS loading", the shear test results of the granite joint with the specimen length of 200 mm under the CNS condition, is depicted in Fig. 8 of "Appendix".

4 Concluding Remarks

A thorough review of the laboratory direct shear testing apparatuses available worldwide for dynamic testing pointed out the inherent limitations in obtaining the mechanical properties of rock discontinuities subject to the authentic seismic wave loads in both the normal and tangential directions. A new shear testing device was therefore developed at the Key Laboratory of Shale Gas and Geoengineering, Institute of Geology and Geophysics, Chinese Academy of Sciences. This equipment has been described in this technical note.

Four new key technologies, which characterize the novel equipment, including dynamic and cyclic loading, servo closed-loop constant normal stiffness loading, multiscale model testing and high-resolution detection, have been presented. These allow the realistic simulation of the strong earthquake wave loading conditions in both the normal and tangential directions.

The new testing device is capable of testing natural and artificial discontinuities, intact rock specimens subject to static or seismic wave loads in a range of shear strain rate of $1\times10^{-6}\sim1\times10^{1}$/s (shear rate of 0.001 ~ 1000 mm/s), frequency of 0 ~ 20 Hz and shear displacement of ± 200 mm, aiming at obtaining the shear strength parameters under both static and dynamic conditions. The results of preliminary shear tests in the static and dynamic conditions have been described to show that the new testing device is stable and allows one to perform tests in a reliable manner, meanwhile, the shear strain rate in the range of $1\times10^{-1}\sim1\times10^{1}$/s (seismic wave loads) has a remarkable influence on the resistance of the joint, and the shear behavior of the joint under the seismic wave loads has a notable difference with its in the quasi static condition.

Acknowledgements We want to remember Prof. Barla, who unexpectedly passed away. This paper was encouraged positively and revised

meticulously by Prof. Barla in the process of its submission. Unfortunately, during the modification of the manuscript after review, the grievous news of Prof. Barla came suddenly and we are all in extreme grief. This article is dedicated to distinguished Prof. Barla to cherish our memory for him. This research was supported with funds from the National Natural Science Foundation of China under Grant Nos. 41825018, 41672307 and the Chinese Academy of Sciences under Knowledge Innovation Project Grant No. KZZD-EW-05-02.

Compliance with Ethical Standards

Conflict of Interest The authors have declared no conflict of interest.

Appendix

To elaborate the key technique of "cyclic loading", an example of cyclic shear test results of the granite joint with the specimen length of 1000 mm (along shear direction), the width of 250 mm and the height of 300 mm under the CNL condition is shown in Fig. 7. The granite joint has the regular sawtooth shape with five identical and isosceles saw teeth, and each one possesses the undulated angle of 13°, the height of 23.09 mm as well as the length of 200 mm, as depicted in Fig. 7a. Fig. 7b–d illustrate the load-displacement-time relations of the cyclic shear test results of the granite joint. From Fig. 7b, c, it can be found that there are three cyclic shear processes, where the shear rate and the normal load remain constant at values of 1 mm/s and 25 kN, respectively, which reveals the reliability of the "cyclic loading" technique. In Fig. 7b, c, it shows that the shear loading amplitude and the frequency are 30 mm and 0.0083 Hz, respectively. It indicates that the shear resistance (the peak shear load) in both the forward positive and backward positive shear processes decreases slightly from the first cycle to the third cycle, as depicted in Fig. 7b, d.

To give a detailed description of the key technique of "CNS loading", an example of shear test results of the granite joint with the specimen length of 200 mm (along shear direction), the width of 100 mm and the height of 150 mm under the CNS condition is depicted in Fig. 8. The granite joint has the tilted flat and straight shape with the inclination angle of 14°, as shown in Fig. 8a. Fig. 8b–d illustrate the load-displacement relations of the shear test results of the granite joint under the CNS condition. According to Fig. 8b, c, it can be found that in CNS tests with the k_n of 0, i.e., CNL tests, the normal load retains constant at the value of 10 kN with the increase of the normal displacement and the shear displacement. In comparison with the k_n of 1.56 kN/mm and 3 kN/mm of CNS tests, the normal load and the normal displacement are well proportioned with the normal displacement increasing at different shear rate values of 0.1 mm/s and 1 mm/s, which reflects the reliability of the "CNS loading" technique. It indicates that the joint shows an elastic-plastic behavior in CNL tests, while the shear load increases gradually with the shear displacement increasing in CNS tests ($k_n = 1.56$ kN/mm and $k_n = 3$ kN/mm), as depicted in Fig. 8d.

References

Barla G, Barla M, Martinotti ME (2010) Development of a new direct shear testing apparatus. Rock Mech Rock Eng 43(1):117–122

Barton N (1973) Review of a new shear-strength criterion for rock joints. Eng Geol 7(4):287–332

Barton N, Choubey V (1977) The shear strength of rock joints in theory and practice. Rock Mech 10(1):1–54

Cen DF, Huang D (2017) Direct shear tests of sandstone under constant normal tensile stress condition using a simple auxiliary device. Rock Mech Rock Eng 50:1425–1438

Crawford AM, Curran JH (1981) The influence of shear velocity on the frictional resistance of rock discontinuities. Int J Rock Mech Min Sci Geomech Abstr Pergamon 18(6):505–515

Dang WG, Konietzky H, Frühwirt T (2016) Direct shear behavior of a plane joint under dynamic normal load (DNL) conditions. Eng Geol 213:133–141

Fathi A, Moradian Z, Rivard P et al (2016) Shear mechanism of rock joints under pre-peak cyclic loading condition. Int J Rock Mech Min Sci 83:197–210

Grasselli G, Egger P (2003) Constitutive law for the shear strength of rock joints based on three-dimensional surface parameters. Int J Rock Mech Min Sci 40(1):25–40

Guo SF, Qi SW (2015) Numerical study on progressive failure of hard rock samples with an unfilled undulate joint. Eng Geol 193:173–182

Hans J, Boulon M (2003) A new device for investigating the hydro-mechanical properties of rock joints. Int J Numer Anal Methods Geomech 27(6):513–548

Hu YX, Liu SC, Dong W (1996) Earthquake engineering. CRC Press, London

Huang D, Zhu TT (2018) Experimental and numerical study on the strength and hybrid fracture of sandstone under tension-shear stress. Eng Fract Mech 200:387–400

Huang D, Zhu TT (2019) Experimental study on the shear mechanical behavior of sandstone under normal tensile stress using a new double-shear testing device. Rock Mech Rock Eng 52(9):3467–3474

Indraratna B, Haque A, Aziz N (1998) Laboratory modelling of shear behaviour of soft joints under constant normal stiffness conditions. Geotech Geol Eng 16(1):17–44

ISRM (2007) The complete ISRM suggested methods for rock characterization, testing and monitoring: 1974–2006. In: Ulusay R, Hudson JA (eds) Suggested methods prepared by the commission on testing methods, international society for rock mechanics, compilation arranged by the ISRM Turkish national group. Kozan Ofset, Ankara

Jiang Y, Xiao J, Tanabashi Y et al (2004) Development of an automated servo-controlled direct shear apparatus applying a constant normal stiffness condition. Int J Rock Mech Min Sci 41(2):275–286

Kleepmek M, Khamrat S, Thongprapha T et al (2016) Displacement velocity effects on rock fracture shear strengths. J Struct Geol 90:48–60

Konietzky H, Frühwirt T, Luge H (2012) A new large dynamic rockmechanical direct shear box device. Rock Mech Rock Eng 45(3):427–432

Li HB, Feng HP, Liu B et al (2006) Experimental studies on mechanical properties of rock joints under dynamic loading. Key Eng Mater 326–328:1709–1712

Li JC, Ma GW, Zhao J (2011) Analysis of stochastic seismic wave interaction with a slippery rock fault. Rock Mech Rock Eng 44(1):85–92

Li JC, Li HB, Jiao YY, Liu YQ, Xia X, Yu C (2014) Analysis for oblique wave propagation across filled joints based on thin-layer interface model. J Appl Geophys 102:39–46

Mehrishal S, Sharifzadeh M, Shahriar K et al (2016) An experimental study on normal stress and shear rate dependency of basic friction coefficient in dry and wet limestone joints. Rock Mech Rock Eng 49(12):4607–4629

Patton FD (1966) Multiple modes of shear failure in rock. In; Proceedings of the 1st Congress of International Society for Rock Mechanics, Lisbon, Portugal, 25 September–1 October. pp. 509–513

Qi SW, Xu Q, Lan HX et al (2010) Spatial distribution analysis of landslides triggered by 2008.5.12 Wenchuan earthquake. China Eng Geol 116:95–108

Qi SW, Xu Q, Zhang B et al (2011) Source characteristics of long runout rock avalanches triggered by the 2008 Wenchuan earthquake, China. J Asian Earth Sci 40:896–906

Qi SW, Lan HX, Dong JY (2015) An analytical solution to slip buckling slope failure triggered by earthquake. Eng Geol 194:4–11

Schneider HJ (1977) The time dependence of friction of rock joints. Bull Int Assoc Eng Geol 16:235–239

Zheng BW, Qi SW (2016) A new index to describe joint roughness coefficient (JRC) under cyclic shear. Eng Geol 212:72–85

Zhu TT, Huang D (2019) Experimental investigation of the shear mechanical behavior of sandstone under unloading normal stress. Int J Rock Mech Min Sci 114:186–194